Optics and Lasers in Engineering 194 (2025) 109173

Contents lists available at ScienceDirect

Optics and Lasers in Engineering

journal homepage: www.elsevier.com/locate/optlaseng

Collimated phase measuring deflectometry II: Re-design of the optical layout for high-curvature surfaces

Corey Austin [a,*], Wanqi Shang [b,c], Lei Huang [a], Tianyi Wang [a], Carl Paterson [f], Peter Török [b,c,d,e], Mourad Idir [a]

[a] National Synchrotron Light Source II (NSLS-II), Brookhaven National Laboratory, P.O. Box 5000, Upton, NY 11973, USA
[b] School of Physical and Mathematical Sciences, Nanyang Technological University, 50 Nanyang Drive, Singapore 639798, Singapore
[c] Singapore Centre for Environmental Life Sciences Engineering (SCELSE), Nanyang Technological University, 60 Nanyang Drive, Singapore 637551, Singapore
[d] Lee Kong Chian School of Medicine, Nanyang Technological University, 59 Nanyang Drive, Singapore 639798, Singapore
[e] Institute for Digital Molecular Analytics and Science (IDMxS), 59 Nanyang Drive, Singapore 639798, Singapore
[f] Blackett Laboratory, Imperial College London, Prince Consort Road, London, SW7 2BW, UK

ABSTRACT

Collimated phase measuring deflectometry (CPMD) is an optical metrology technique developed to improve upon traditional phase measuring deflectometry (PMD). CPMD utilizes telecentric imaging and collimated structured light illumination to eliminate the height-slope ambiguity present in traditional PMD measurements. After the publication of the first CPMD paper, efforts began to optimize the optical layout of the CPMD system. The first proposed change, and the one detailed in this work, was to move the Fourier transform (FT) lens closer to the surface under test (SUT). Moving the FT lens closer to the SUT meant that for a given FT lens diameter, a larger range of surface slopes on the SUT could be measured. This change to the optical layout was not trivial and introduced at least two concerns that had to be addressed: telecentricity in the imaging path and possible ghost reflections from the re-located FT lens. In this work, we examine how these concerns were addressed and present results showing that the revised optical layout is capable of measurement results at least as good as the original CPMD optical layout. We also demonstrate the increased slope measuring range of the revised optical layout.

1. Introduction

In traditional phase measuring deflectometry (PMD) systems, precise calibration of the camera is critical to making error-free measurements [1–7]. This calibration relies heavily on precise knowledge of the relative positions of the components in the system in order to accurately map between screen pixels and camera pixels. Any errors in component positioning lead to camera calibration errors which lead directly to measurement errors. The technique of collimated phase measuring deflectometry (CPMD) introduces telecentric imaging to greatly reduce errors in the camera calibration process. The camera rays in a CPMD system are parallel to the optical axis and their lateral coordinates on the surface under test (SUT) are not affected by sample depth [8].

Additionally, traditional PMD measurements are subject to the problem of height-slope ambiguity [9–15,1]. This height-slope ambiguity is present because different slopes placed at different sample depths can yield rays that land at the same location on the screen. With CPMD, a Fourier transform (FT) lens is used to mitigate the height-slope ambiguity. An FT lens maps the field angle of rays before the lens to distinct positions in the image plane. This means that surface slopes can be uniquely determined, even if the SUT is placed at a depth different from the reference plane [8].

The CPMD system described in [8] utilized the optical layout that is represented in Fig. 1(a). In this layout, FT lens is placed on the screen side of the beamsplitter. This arrangement worked well and allowed the illumination and imaging paths to function without sharing optical components. However, as the slope range of the surfaces under test became larger, the FT lens became the limiting aperture of the system. In order to increase the slope measuring range of the system without needing to increase the size of the FT lens, a change to the optical layout of the system was proposed. In the new layout, shown in Fig. 1(b), the FT lens is moved to the other side of the beamsplitter and thus closer to the SUT. In this work, we examine how this change to the optical layout increases the slope measuring range, we address the challenges associated with the optical layout change, we compare measurement results between the two optical layouts, and finally, we present results demonstrating the increased slope measuring range.

* Corresponding author.
E-mail address: caustin@bnl.gov (C. Austin).

https://doi.org/10.1016/j.optlaseng.2025.109173
Received 24 April 2025; Received in revised form 12 June 2025; Accepted 15 June 2025
Available online 23 June 2025

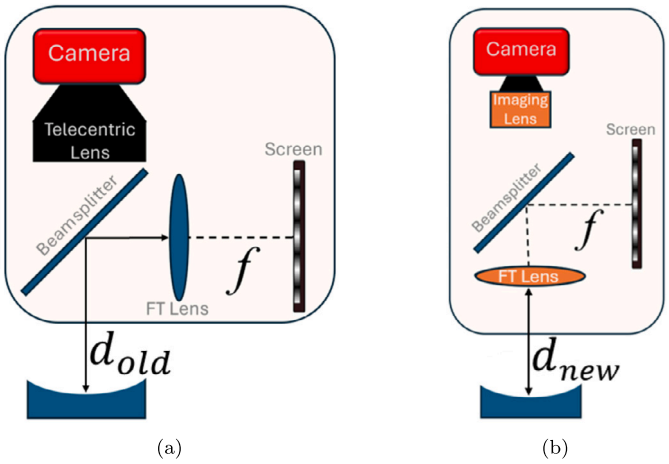

Fig. 1. (a) Original and (b) revised CPMD layouts. The revised layout features a reduced distance, d_{new}, between the surface under test and the Fourier transform (FT) lens. This increases the measurable slope range of the CPMD system by increasing the acceptance angle of the FT lens.

2. CPMD system re-design

In order to increase the slope measuring range of the CPMD system, a change to the optical layout of the system was proposed: move the FT lens closer to the SUT. If we consider a fan of rays leaving the SUT, as the distance from the SUT increases, the diameter of the fan of rays also increases. The FT lens must capture all of these rays in order to measure the full SUT, so as the separation distance between SUT and FT lens is increased, the minimum diameter of the FT lens must also increase. In the case of a spherical concave mirror, we can state the relationship between the separation distance and the minimum diameter with the following equation:

$$D_{lens} = \begin{cases} 2d\tan(\theta) - D_{SUT}, & \text{if } d \geq 2f_{SUT} \\ D_{SUT}, & \text{otherwise} \end{cases} \quad (1)$$

where D_{lens} is the FT lens minimum diameter, d is the separation distance between the SUT and FT lens, θ is the max field angle (twice the maximum slope), D_{sut} is the diameter of the surface under test, and f_{SUT} is the focal length of the SUT. The FT lens diameter, D_{lens}, in all cases must be equal to or greater than the SUT diameter, D_{sut} due to the use of telecentric imaging. In the original CPMD layout, the minimum distance between the FT lens and the SUT is 185 mm due to the space required by the beamsplitter and the mechanical mounting hardware of the beamsplitter and FT lens. In the revised CPMD layout, the minimum distance between the FT lens and SUT can be less than 10 mm.

In the example illustrated in Fig. 2, a 50 mm diameter concave mirror with a 100 mm radius of curvature and total slope range of just over ± 260 mrad serves as the SUT. Using the equation above, we can see that measuring this mirror with the original CPMD optical layout would require an FT lens with a minimum diameter of 164 mm. With the revised setup, this same measurement could be made with a 50 mm diameter Fourier lens.

2.1. Potential issues with re-design

We can consider the CPMD system as consisting of two optical paths: the illumination path and the imaging path. The illumination path consists of the screen, FT lens, beamsplitter, and SUT. The components in this path do not change when the FT lens is moved, so this path is not affected by the proposed change to the optical layout. The imaging path in the original CPMD layout consisted of the camera, telecentric lens, beamsplitter, and SUT. Moving the FT lens to the other side of the beamsplitter means that the FT lens is now in the imaging path. The fundamental principles of CPMD require that the camera rays in the imaging path be collimated [8]. Previously, this was achieved by the use of a commercial telecentric lens. We must consider how adding an optical element to this path affects telecentricity and ensure that the imaging path remains telecentric and thus the camera rays remain collimated. Additionally, placing the FT lens in the imaging path means that there is a direct path for ghost reflections from the lens to travel back to the camera. These ghost reflections could influence the ability to make measurements and must also be addressed. Finally, we must consider that having the FT lens in both the illumination and imaging paths means that any aberrations introduced by the FT lens will now be present in both optical paths.

2.2. Addressing telecentricity

A telecentric lens has the entrance pupil, exit pupil, or both located at infinity and these three types of telecentric lenses are referred to as object space telecentric, image space telecentric, or bi-telecentric, respectively. The result of having the pupil at infinity is that the chief rays in the respective space are parallel to the optical axis and can be considered collimated [16].

As an example, we can consider an object space telecentric lens. With the entrance pupil located at infinity, the object space chief rays are parallel to the optical axis. An object space telecentric lens will see no magnification change as the object distance is changed. Object space and bi-telecentric lenses are often used in machine vision inspection applications where the sample depth of the part being examined may vary from part to part [17]. CPMD utilizes object space telecentricity to make the lateral coordinates of the camera rays on the SUT independent of the placement of the SUT along the optical axis.

The original CPMD layout used an off-the-shelf bi-telecentric lens from Edmund Optics (EO #55-348). The camera rays leaving this telecentric lens were collimated, and practically no change in magnification could be seen when the SUT was moved along the optical axis. The proposed re-design moves the FT lens to a location between the telecentric lens and the SUT. Moving the FT lens to this new location results in the loss of telecentricity because the FT lens will bring the collimated camera rays to a focus.

To avoid losing telecentricity and maintain collimated camera rays, we proposed replacing the telecentric lens with a traditional imaging lens and using it along with the FT lens to form a compound lens. By spacing the FT and imaging lenses properly along the optical axis, it is possible to place the combined focus of the FT lens and the front half of the imaging lens at the location of the aperture stop in the imaging lens. We constructed a Zemax [18] model to determine the optimal spacing and placed the elements onto an optical table at the prescribed spacing. We then performed measurements to refine the spacing and to confirm telecentric imaging.

2.2.1. Modeling telecentricity

To model telecentricity in the imaging path, we created a Zemax model which consisted only of the object, FT lens, imaging lens, and image. We created a merit function that minimized the angle between the optical axis and the chief rays leaving the object by adjusting the spacing between the FT lens and imaging lens. To choose the lenses, two main factors were considered.

First, the focal length of the FT lens was chosen to be around 500 mm. This was driven by the illumination path. The mapping between the field angle of rays reflected from the SUT and their position on the monitor displaying the fringe patterns is:

$$y = f\tan\theta \quad (2)$$

where y is the position on the monitor, f is the focal length of the FT lens, and θ is the field angle. To ensure that we could map the total proposed slope range of ± 200 mrad to the monitor, we selected an FT lens (Edmund Optics 86084) with a focal length of 494.72 mm. If

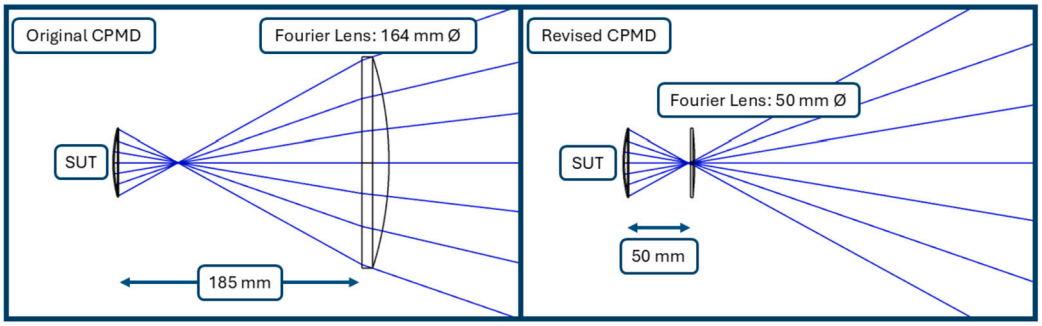

Fig. 2. Measuring a 50 mm diameter SUT with 100 mm radius of curvature using the original CPMD optical layout would require a 164 mm diameter FT lens. The revised CPMD optical layout is able to perform this same measurement with only a 50 mm diameter FT lens.

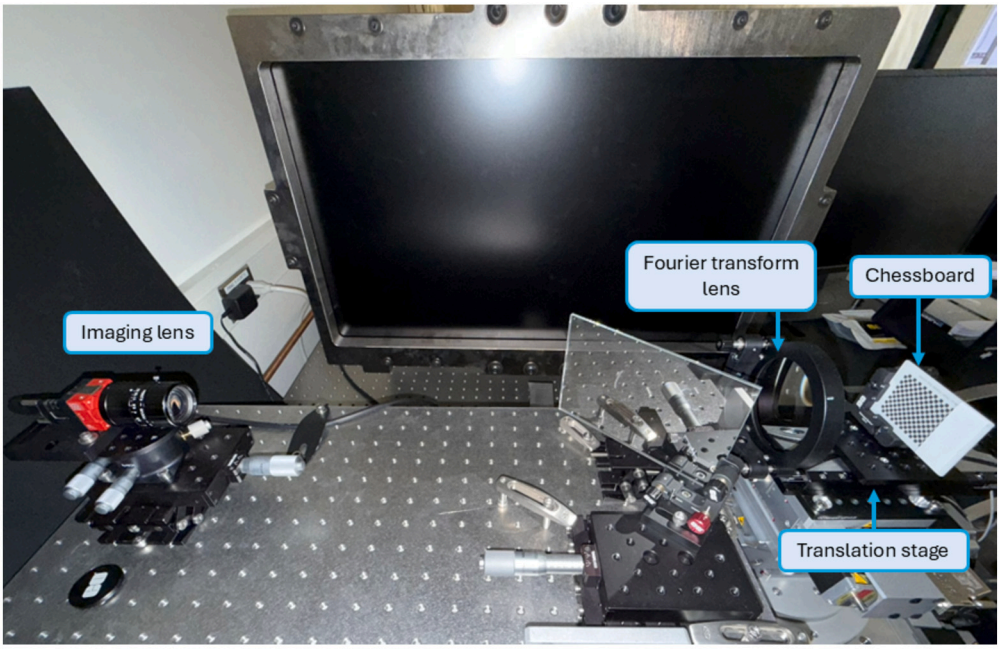

Fig. 3. Photograph of the experimental setup used to test telecentricity in the imaging path. A calibration chessboard is placed on a translation stage which is moved along the optical axis to positions ± 15 mm from the home position. The telecentricity of the FT lens + imaging lens combination is calculated by comparing the location of the chessboard vertices in images captured at both locations.

we consider a 50 mm diameter concave mirror with maximum surface slopes of ± 200 mrad (giving maximum field angles of ± 400 mrad), the maximum screen positions are approximately ± 184 mm from the center of the screen. The monitor used to display the fringe patterns in our experimental setup is 693 mm x 393 mm, so we are able to measure the full slope range and avoid any possible effects from the edge of the monitor.

The second consideration was to utilize as many of the camera pixels as possible. To achieve this goal, we needed to select an imaging lens with a field of view slightly larger than the FT lens when the two lenses are optimally spaced for telecentric imaging. This required iterating between telecentricity model mentioned above and a second Zemax model that determined the object height for a given image height and separation distance. The camera in the CPMD setup uses a sensor that is 7.8 mm x 7.8 mm, so we fixed the image height to 7.8 mm and spaced the object and image at the separation distance determined by the telecentricity model. With the image height and separation distance fixed, the object height could be determined to provide the field of view information required. Ultimately, we selected a lens with a fixed focal length of 50 mm (Edmund Optics 59873).

With both lenses selected, the optimal spacing between lenses was determined to be around 494.7 mm. We placed the lenses on an optical table at approximately the correct distance and performed the measurements described in the following section to maximize the telecentricity of the imaging path.

2.2.2. *Measuring telecentricity*

To confirm that the camera rays of the revised optical layout were indeed collimated, we measured the change in magnification as a target was moved along the optical axis. For this measurement, a calibration checkerboard was placed on an axial translation stage at the location where a SUT would be placed. The translation stage was moved ± 15 mm along the optical axis from the home position and images of the checkerboard were captured at each end location. A photograph of the experimental setup used to measure telecentricity is shown in Fig. 3.

Using OpenCV [19] and Python, the vertices of the checkerboard were identified in the captured images and the positions of the vertices at the two axial distances were compared. The measurement was performed first using the commercial telecentric lens from the original CPMD setup and then repeated with the FT lens + imaging lens from the revised optical layout. For the FT lens + imaging lens, the spacing along the optical axis between the two lenses was adjusted to minimize the change in magnification. Both measurements showed the locations of the checkerboard vertices varying by less than one camera pixel. The maximum pixel error for the commercial telecentric lens was 0.76 pixels and for the FT + imaging lens, the maximum error was 0.08 pixels

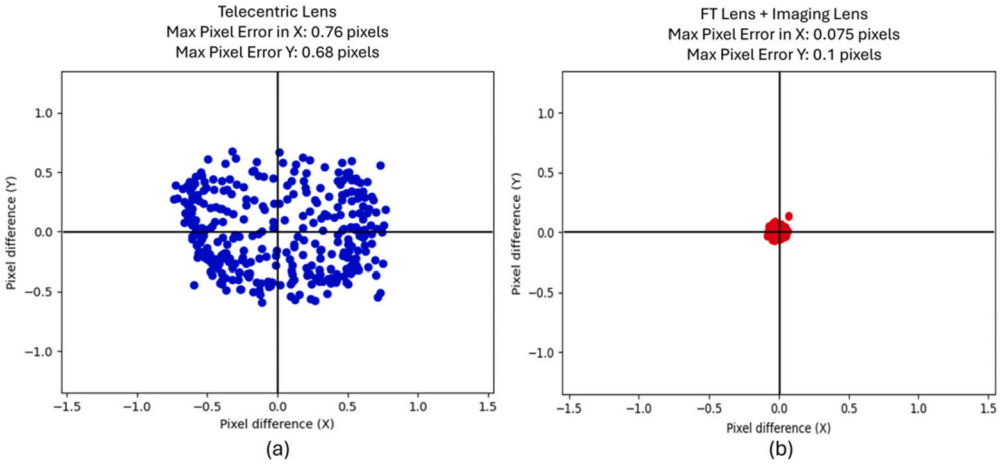

Fig. 4. Plot comparing the change in magnification as a checkerboard target is translated 30 mm along the optical axis. The locations of the checkerboard vertices are identified in images taken at either end of the translation and the difference in pixels is measured. Results are shown for the commercial telecentric lens (a) and for the T lens + imaging lens (b).

as shown in Fig. 4. The experiment demonstrated that the FT + imaging lens combination offered equivalent, or even slightly improved telecentricity when compared with the commercial telecentric lens used in the original CPMD setup. The slightly improved telecentricity is likely due to having a smaller aperture in the imaging lens compared to the commercial telecentric lens. The range over which the telecentricity was tested (± 15 mm) is far greater than the range needed for mirror measurements, so the difference is not likely to affect or improve measurement results.

2.3. Addressing ghost reflections

In the original CPMD optical layout, the FT lens was not within the field of view of the camera. In the revised layout, the FT lens lies fully within the field of view of the camera. The reflectance of uncoated glass is around 4% which means that both the front and back surfaces of the FT lens could potentially reflect the fringe patterns displayed on the monitor back towards the camera. Images of the first order ghost reflections can be captured by the camera by placing a dark background behind the lens in place of a reflective SUT. These images of the ghost reflections can then be subtracted from subsequent measurements of the SUT. The second order reflections, however, include reflections from the SUT and change based on the SUT and cannot be subtracted. With sufficient intensity, these second order reflections can introduce errors into the CPMD measurements.

We can calculate the relative intensity of the ghost images reflected from the surfaces of the FT lens. When light is reflected from the lens, we multiply by the reflectance of the lens, R_{lens} to obtain the relative intensity of the reflected light. For each transmission through the glass, T_{glass}, we multiply by $1 - R_{glass}$. We also need to take into account the reflectance of the SUT, R_{SUT}, in order to consider higher order ghost reflections. In the example that follows, we used a mirror from Edmund optics with an enhanced aluminum coating which has an average reflectance, R_{mirror}, of > 95% [20].

For an uncoated FT lens, the relative intensity of the first order reflections from the front (the side of the lens facing the camera) and rear of the lens are, respectively:

$$I_{front,1st} = 1 \cdot R_{lens} = 0.04 \tag{3}$$

$$I_{rear,1st} = 1 \cdot T_{lens} \cdot R_{lens} \cdot T_{lens} = 0.037 \tag{4}$$

The second order reflections from the front and rear of the lens, respectively, are then:

$$I_{front,2nd} = 1 \cdot T_{lens}^2 \cdot R_{mirror} \cdot T_{lens} \cdot R_{lens} \cdot T_{lens} \cdot R_{mirror} \cdot T_{lens}^2 = 0.028 \tag{5}$$

Table 1
Relative intensity of 1st and 2nd order ghost reflections from the front and rear of both uncoated and AR coated FT lenses.

Surface	Order	Uncoated	Vis 0°
Front	1st	0.0400	0.00400
Rear	1st	0.0369	0.00397
Front	2nd	0.0283	0.00352
Rear	2nd	0.0307	0.00355

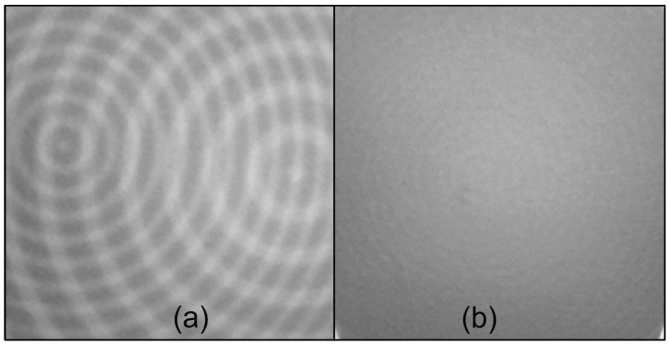

Fig. 5. Comparison of ghost images captured using the (a) uncoated Fourier lens and (b) Vis 0° AR coated FT lens [21]. A concentric fringe pattern was displayed on the monitor and the FT lenses were intentionally misaligned to separate the front and back ghost reflections. Both images were captured with the same camera exposure settings.

$$I_{rear,2nd} = 1 \cdot T_{lens}^2 \cdot R_{mirror} \cdot R_{lens} * R_{mirror} \cdot T_{lens}^2 = 0.0307 \tag{6}$$

We can now make these same calculations for an FT lens with an anti-reflective (AR) coating (Edmund Optics Vis 0° [21]) with a reflectance of 0.4%. The results are summarized in Table 1 and show that the AR coating on the FT lens reduces the relative intensity by approximately a factor of 10.

Initial testing with an uncoated FT lens indicated that the intensity of the ghost reflections captured by the camera was enough to influence measurement results. For the first order reflections, background subtraction was effective in limiting the effect, but the second order reflections had sufficient intensity to affect the measurement results. To address the ghost reflections, we replaced the uncoated FT lens with a Vis 0° AR coated lens. For comparison, we captured images of the first order ghost reflections from the two lenses using the same camera exposure settings. Fig. 5 compares the ghost images from the uncoated and coated lenses

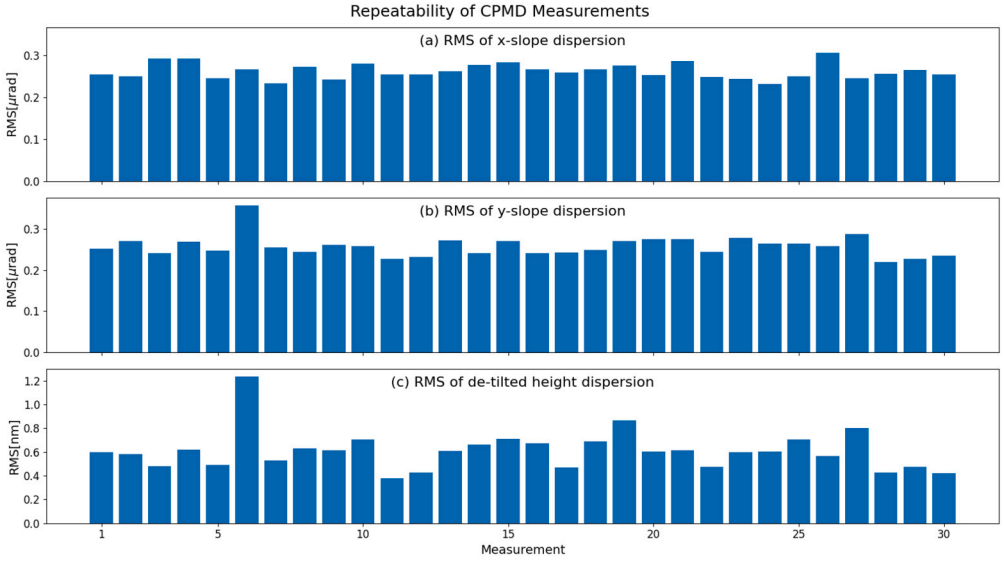

Fig. 6. Repeatability of CPMD measurements with the re-designed optical layout. (a) X-slope and (b) y-slope are repeatable to a level better than 0.5 μrad and (c) height is repeatable to a level better than 1.2 nm.

and it shows that the intensity of the ghost reflections is greatly reduced. Subsequent measurements of mirrors demonstrated that the change to an AR coated FT lens was sufficient to reduce the intensity of the ghost reflections to a level that no longer interfered with the measurement ability of the CPMD system when considering reflective optics. For non-reflective optics such as lenses, the decreased reflectivity of the SUT is closer to the reflectivity of the FT lens so the relative intensity of the ghost reflections is increased. For reflective optics, we have shown that the relative intensity of the ghost reflections is small enough to not interfere with the measurement accuracy of the system, but for non-reflective optics, we will need to consider the trade-off between slope measuring range and intensity of ghost reflections.

3. Experimental evaluation

The next step for the validation of the revised CPMD optical layout was to measure mirrors that were measured with the original CPMD optical layout and compare the results. As with the original CPMD optical layout, camera calibration is a critical step that must be completed prior to making measurements. This calibration process is needed to accurately convert from camera pixels to distances on the SUT. In the revised layout, the combined FT lens + imaging lens functions in the same way as the telecentric lens functioned in the original optical layout, so the camera calibration process is identical and the process was completed without any difficulties. While making measurements with the revised optical layout, we found that the boundary between the edge of the mirrors and the holder that we used for the evaluation created spurious reflections that interfered with the measurements. Because of this, we reduced the area of interest to a circle of 30 mm diameter instead of the full 50 mm diameter of the mirror. Nonetheless, the results from the revised layout described in the following sections compared favorably to the results from the original layout and we will continue developing the system using the revised layout including addressing the issues with the mirror holder.

3.1. Repeatability

The first test we performed was to evaluate the repeatability of measurements made with the CPMD system using the revised optical layout. We measured a flat mirror and repeated the measurement 30 times. We then took the mean of these measurements and calculated the dispersion from the mean for each of the individual measurements. We found that both the x-slope and y-slope measurements were repeatable to a level better than 0.5 μrad and the height was repeatable to a level better than 1.2 nm. Fig. 6 is a plot showing the results of the repeatability measurement.

3.2. Sample depth testing

One of the key advantages of CPMD when compared to traditional PMD methods is its greatly reduced sensitivity to sample depth positioning along the optical axis. To evaluate the sensitivity to sample depth positioning, we measured mirrors at their nominal position along the optical axis and then repeated the measurements as the sample was moved along the optical axis using a translation stage. Prior to mounting the mirror on the translation stage, we used the checkerboard from the telecentricity test to align the translation stage to the optical axis to ensure that the motion was along the axis and did not introduce additional errors. Two measurements were made at the nominal position with one serving as the reference measurement for all other measurements and the other serving as a comparison to the reference at the nominal position. As in the original CPMD publication, the mirrors were measured at 1 mm increments up to ± 5 mm from their nominal position.

A flat mirror was measured first and the results from those measurements are shown in Fig. 7. The maximum x-slope deviation was 2.4 μrad RMS and the maximum y-slope deviation was 1.6 μrad RMS. The height measurement showed a maximum deviation from the reference measurement of 6.4 nm RMS.

A mirror with 200 mm radius of curvature (Edmund Optics #13-069) was then measured and those results are shown in Fig. 8. The maximum x- and y-slope deviations from nominal were 8.5 μrad RMS and 6.8 μrad RMS, respectively. For the height reconstruction, the maximum deviation from nominal was 19.3 nm RMS. We do see, as in the original CPMD publication, spherical aberration contributing to the error term as the mirror is translated along the optical axis. Spherical aberration cannot be avoided with the spherical, plano-convex FT lens currently being used, but we plan to address this going forward with a optimized custom FT lens design to include an aspherical surface.

As mentioned previously, the diameter of the measured area was smaller with the revised optical layout due to an issue with the mirror holder, so we re-evaluated the results from [8] using the central 30 mm diameter area as the test area. For the flat mirror, the maximum height error using the central 30 mm diameter in the original setup was found to be 2.0 nm RMS compared to the 6.4 nm RMS height error seen in

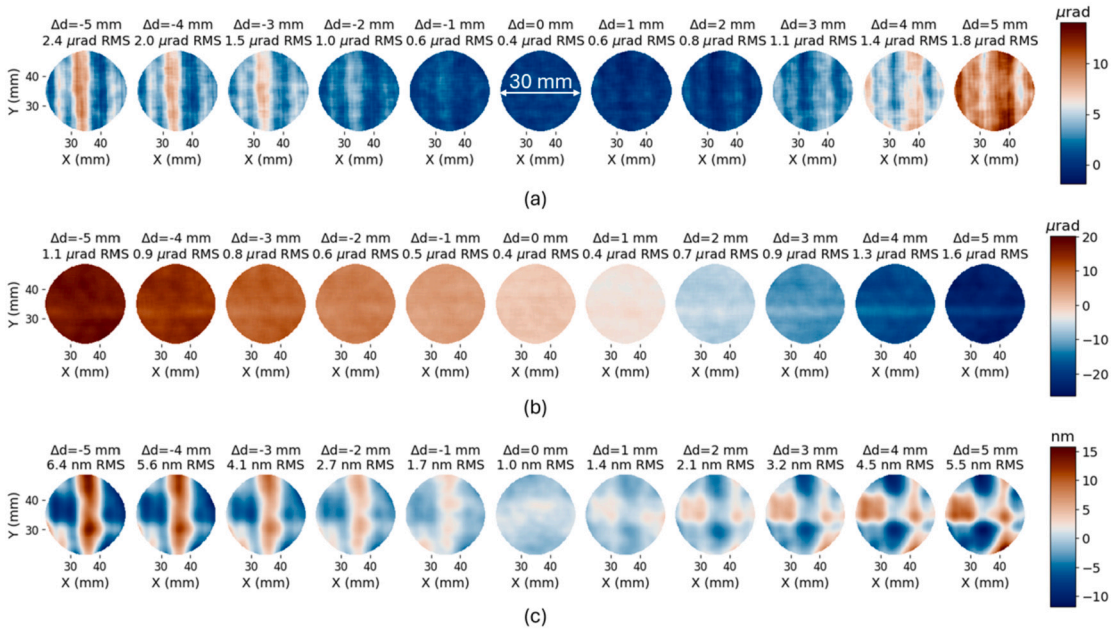

Fig. 7. Measured dispersions of a flat mirror measured at different sample depths. Measured (a) x-slope, (b) y-slope, and (c) height are largely insensitive to depth changes along the optical axis.

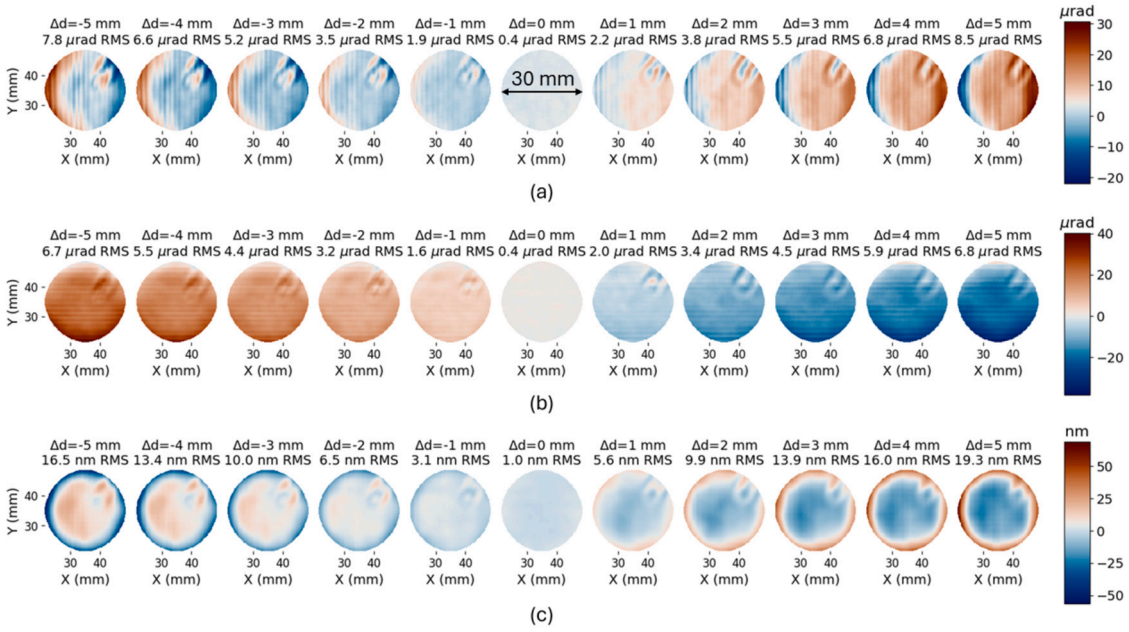

Fig. 8. Measured dispersions of a mirror with 200 mm radius of curvature measured at different sample depths. Measured (a) x-slope, (b) y-slope, and (c) height are largely insensitive to depth changes along the optical axis.

the new setup. For the 200 mm radius of curvature mirror, the original setup showed a maximum height error of 14.5 nm RMS compared to a maximum height error of 19.3 nm RMS in the revised setup. The slight increase in measurement error is likely due to the decreased diameter of the FT lens in the new setup and aberrations present in the yet-to-be optimized imaging path utilizing the imaging lens ± FT lens as a telecentric lens. We are confident that the slight increase in RMS height error can be reduced with optimization of the system and will proceed with development of the revised optical layout.

We also wanted to verify the increased slope measuring range of the revised optical layout by measuring a mirror similar to the one described in the example given in Section 2. For this, we measured a 50 mm diameter mirror with 100 mm radius of curvature (Edmund Optics #13-068). An example of the fringe patterns captured during this measurement is shown in Fig. 9 and the results of this measurement are shown in Fig. 10. We were able to measure a total x-slope range of 456 mrad and a total y-slope range of 373 mrad with a 75 mm diameter FT lens. For comparison, the original CPMD optical layout would have required a 131 mm diameter FT lens to make the same measurement (based on the total x-slope range).

For prototyping and testing of the revised optical layout, we re-used the 145 mm × 100 mm plate beamsplitter (Knight Optical BGF14507) from the original optical layout. With the revised optical layout, this beamsplitter became the limiting aperture of the system as we increased the curvature of the SUT. As the curvature of the mirror is increased, the fan of camera rays leaving the SUT spreads out faster than it would with

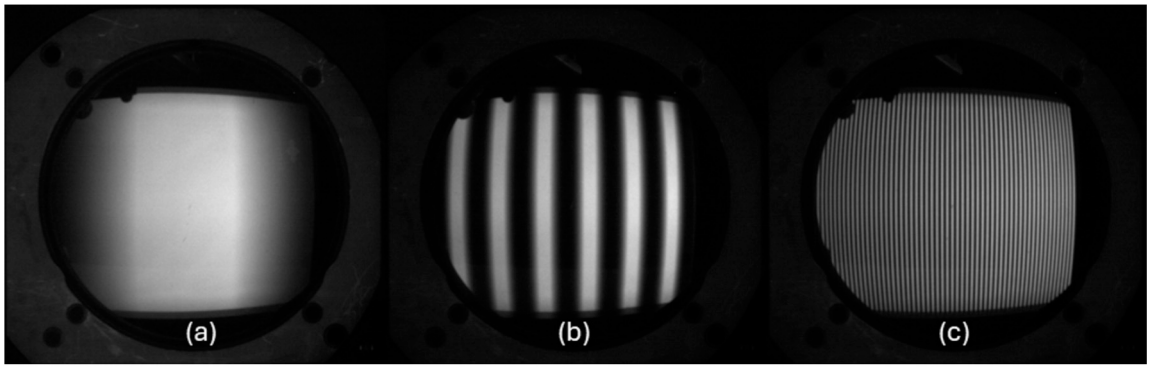

Fig. 9. An example of the fringe patterns captured by the system during measurement of a mirror with 100 mm radius of curvature. The number of fringes displayed on the screen for each captured image were, respectively, (a) 1 fringe, (2) 9 fringes, and (3) 81 fringes.

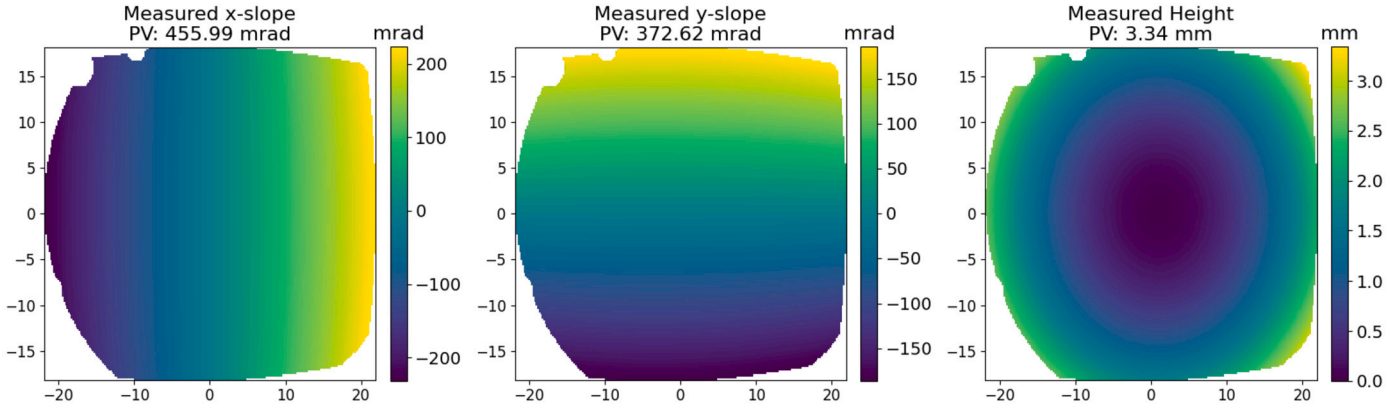

Fig. 10. A 50 mm diameter mirror with 100 mm radius of curvature was measured using the revised optical layout. The measured (a) x-slope and (b) y-slope are shown along with the (c) reconstructed height. Re-using the beamsplitter from the original optical layout limited the measurement area to what is shown. Even with this limitation, the maximum measured slope range was 456 mrad.

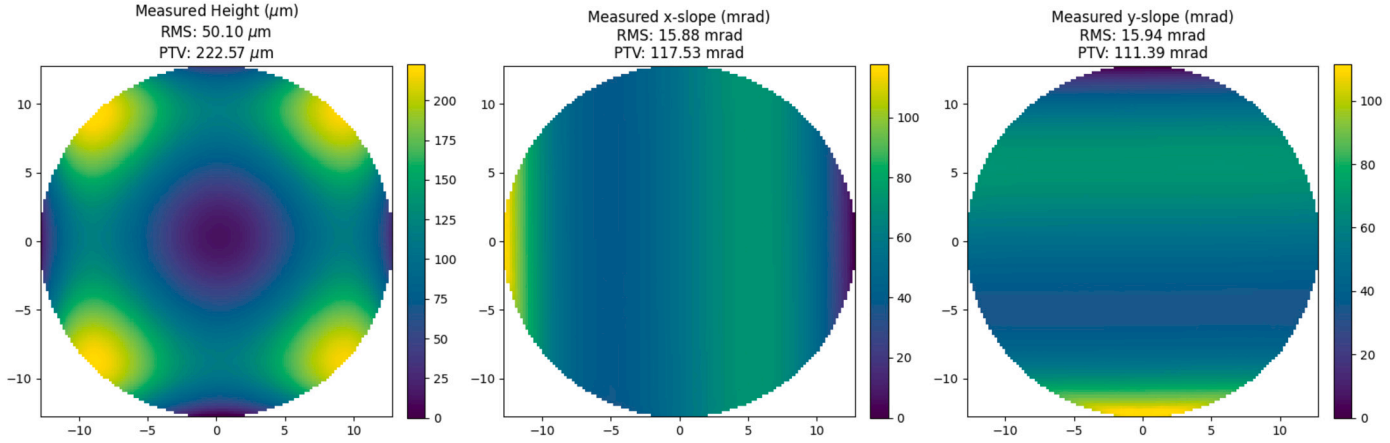

Fig. 11. A freeform mirror with 26 mm clear aperture was measured with the system. The reconstructed height, measured x-slope, and measured y-slope are shown in the panels from left to right. The maximum measured slope range was 117 mrad.

a flatter mirror, and in the case of the 100 mm radius of curvature mirror, some of the camera rays leaving the SUT followed a path that took them beyond the extent of the beamsplitter. This was an expected and accepted trade-off of the optical layout re-design since larger beamsplitters are available as commercial off-the-shelf parts (such as Edmund Optics #72-502). The FT lens, on the other hand, will ultimately need to be a custom design to achieve the best measurement results and a smaller diameter custom FT lens will be less costly and take less time to manufacture. Even with the limiting aperture of the beamsplitter, we can see that the slope measuring range of the system has been increased.

Finally, we sought to verify the ability of the system to measure a freeform mirror that included both convex and concave shapes. The freeform prescription is proprietary, but we are able to share the results of the measurement as shown in Fig. 11. The maximum measured slope range was 117 mrad in the x-direction and 111 mrad in the y-direction.

4. Discussion and conclusion

CPMD is an innovative technique that improves upon traditional PMD methods by reducing or eliminating both the sensitivity to sample

depth positioning along the optical axis and the height-slope ambiguity. This is accomplished by utilizing telecentric imaging to reduce the sensitivity to sample depth positioning and by utilizing a Fourier transform lens to map the field angles of camera rays reflected from the surface under test to positions on the screen displaying fringe patterns.

A change to the optical layout of the components in the CPMD system was proposed in order to increase the slope measuring range of the system for a given FT lens diameter. By moving the FT lens closer to the SUT, the acceptance angle of the FT lens is increased, thus increasing the range of surface slopes that can be measured by the system. While changing the optical layout had the potential to increase the slope measuring range, we also needed to ensure that the measurement accuracy of the system was not affected.

In order to maintain telecentricity in the imaging path, the commercial telecentric lens used in the original CPMD optical layout was replaced with a traditional imaging lens. By carefully spacing the imaging and FT lenses along the optical axis so that the combined focus of the FT lens and the front half of the imaging lens is located at the aperture stop of the imaging lens, we were able to achieve telecentricity at least as good as, if not better than, the telecentricity obtained with the commercial telecentric lens.

Another issue with the potential to affect the measurement accuracy of the system was the introduction of ghost reflections from the surfaces of the FT lens. If the fringe patterns displayed on the screen reflected from the surfaces of the FT lens and had sufficient intensity to be captured by the camera, then the measurement results would be influenced. We found that using an FT lens with an anti-reflective coating reduced the relative intensity of the ghost reflections sufficiently to not affect the measurement ability of the system for reflective optics. If we wish to measure non-reflective optics, we will need to consider the trade-off between the increased slope measuring range and the increased relative intensity of the ghost reflections when compared to the original optical layout. We also found that background subtraction of the first-order ghost reflections is possible, but thus far has not been necessary to maintain measurement integrity.

We next wanted to verify that the changes to the optical layout did not affect the measurement accuracy of the CPMD system. We did this by repeating some of the measurements made in the original CPMD publication. For these measurements, the slope of mirrors was measured with the system and the height of the mirrors was reconstructed from the slope measurements. The first of the measurements verified the repeatability of the system by measuring a flat mirror placed at the nominal sample depth position repeatedly. We found that the repeatability achievable with the revised optical layout was comparable to the repeatability achieved with the original optical layout. The next measurements verified that the system is relatively insensitive to sample depth positioning along the optical axis. Both a flat mirror and a mirror with a 200 mm radius of curvature were measured at the nominal position along the optical axis and the measurements were repeated as the mirrors were translated $\pm$ 5 mm along the optical axis. Again, the performance of the revised optical layout was comparable to that of the original optical layout.

Finally, we wanted to verify the increased slope measuring range of the system. We measured a 50 mm diameter mirror with 100 mm radius of curvature and were able to measure a maximum total slope range of 456 mrad using a 75 mm diameter FT lens. Performing this same measurement with the original optical layout would have required, at minimum, a 131 mm diameter FT lens. Overall, the optical layout redesign achieves the goal of increasing the slope measuring range of the CPMD system and does so without sacrificing measurement accuracy.

Going forward, we have identified three sources of measurement error that, if properly addressed, can improve the measurement accuracy of the system. The first is the presence of spherical aberration mentioned both in the first CPMD publication and also noted here in the section discussing the sample depth testing results. Currently, the FT lens is a singlet, plano-convex spherical lens and spherical aberration cannot be avoided when using this lens. Replacing the spherical lens with an aspherical lens could address this issue, but it must also be balanced with the next source of error which is $f\tan(\theta)$ distortion. As shown in Equation (2), the relationship between the field angle of camera rays reflected from the SUT and the mapping to pixels on the screen is paramount to achieving accurate measurement results. Distortion introduces errors into this mapping relationship with the error increasing as the surface slope (and thus field angle) increases. Optimization of the FT lens to reduce spherical aberration and distortion will increase the measurement accuracy of the CPMD system. Any optimization of the FT lens must also consider how the lens and any aberrations introduced by the lens might affect the imaging path. The final source of error currently being considered is retrace error. Retrace error decreases measurement accuracy as rays taking different paths through the optical elements of the system will accumulate different levels of error due to both the presence of aberrations inherent in the optical design as well as the presence of fabrication anomalies that cannot be avoided. Efforts are underway to implement retrace error calibration methods similar to those used in coherence scanning interferometry [22] in order to reduce the effect on measurement accuracy.

CRediT authorship contribution statement

Corey Austin: Writing – review & editing, Writing – original draft, Visualization, Validation, Software, Methodology, Investigation, Formal analysis, Data curation, Conceptualization. **Wanqi Shang:** Writing – review & editing, Validation, Formal analysis, Conceptualization. **Lei Huang:** Writing – review & editing, Validation, Supervision, Resources, Project administration, Methodology, Investigation, Funding acquisition, Conceptualization. **Tianyi Wang:** Writing – review & editing, Conceptualization. **Carl Paterson:** Writing – review & editing, Supervision. **Peter Török:** Writing – review & editing, Supervision. **Mourad Idir:** Writing – review & editing, Supervision, Resources, Project administration, Funding acquisition, Conceptualization.

Funding

This work was supported by Brookhaven National Laboratory (BNL LDRD 25-024), the NSLS-II Facility Improvement Project (21153), U.S. Department of Energy Office of Science (DE-SC0012704), and the Accelerator and Detector Research Program, part of the Scientific User Facility Division of the Basic Energy Science Office of the U.S. Department of Energy, under the Field Work Proposal No. FWP-PS032.

Declaration of competing interest

The authors declare that they have no known competing financial interests or personal relationships that could have appeared to influence the work reported in this paper.

Acknowledgement

The authors want to thank Philip Boccabella in the Research & Development Group of NSLS-II for the mechanical machining. This research used resources of the National Synchrotron Light Source II, a U.S. Department of Energy Office of Science User Facility, operated for the DOE Office of Science by Brookhaven National Laboratory under Contract No. DE-SC0012704. Thanks are also extended to the funding from National Research Foundation Singapore (NRF-CRP24-2020-0001).

Data availability

Data will be made available on request.

References

[1] Olesch E, Faber C, Häusler G. Deflectometric self-calibration for arbitrary specular surfaces. In: Proc. DGao; 2011.

[2] Xiao Y-L, Su X, Chen W. Flexible geometrical calibration for fringe-reflection 3d measurement. Opt Lett 2012;37(4):620–2. https://doi.org/10.1364/OL.37.000620. https://opg.optica.org/ol/abstract.cfm?URI=ol-37-4-620.

[3] Han H, Wu S, Song Z. An accurate calibration means for the phase measuring deflectometry system. Sensors 2019;19(24). https://doi.org/10.3390/s19245377. https://www.mdpi.com/1424-8220/19/24/5377.

[4] Xu X, Zhang X, Niu Z, Wang W, Zhu Y, Xu M. Self-calibration of in situ monoscopic deflectometric measurement in precision optical manufacturing. Opt Express 2019;27(5):7523–36. https://doi.org/10.1364/OE.27.007523. https://opg.optica.org/oe/abstract.cfm?URI=oe-27-5-7523.

[5] Allgeier S, Gengenbach U, Köhler B, Reichert K-M, Hagenmeyer V. Reproducibility of two calibration procedures for phase-measuring deflectometry. In: Morris MBN, Creath K, Porras-Aguilar R, editors. Interferometry XX. International society for optics and photonics, vol. 11490. SPIE; 2020. p. 114900G.

[6] Wang R, Li D, Zhang X. Systematic error control for deflectometry with iterative reconstruction. Measurement 2021;168:108393. https://doi.org/10.1016/j.measurement.2020.108393.

[7] Huang L, Idir M, Zuo C, Asundi A. Review of phase measuring deflectometry. Opt Lasers Eng 2018;107:247–57. https://doi.org/10.1016/j.optlaseng.2018.03.026.

[8] Huang L, Wang T, Austin C, Lienhard L, Hu Y, Zuo C, et al. Collimated phase measuring deflectometry. Opt Lasers Eng 2024;172:107882. https://doi.org/10.1016/j.optlaseng.2023.107882.

[9] Graves LR, Choi H, Zhao W, Oh CJ, Su P, Su T, et al. Model-free deflectometry for freeform optics measurement using an iterative reconstruction technique. Opt Lett 2018;43(9):2110–3. https://doi.org/10.1364/OL.43.002110. https://opg.optica.org/ol/abstract.cfm?URI=ol-43-9-2110.

[10] Yue H-M, Wu Y-X, Song Y-P, Liu Y. Solution to the slope-height ambiguity problem in phase measuring deflectometry based on a co-axial telecentric optical path. Meas Sci Technol 2020;31(4):045007. https://doi.org/10.1088/1361-6501/ab472f.

[11] Petz M, Tutsch R. Reflection grating photogrammetry: a technique for absolute shape measurement of specular free-form surfaces. In: Stahl HP, editor. Optical manufacturing and testing VI. International society for optics and photonics, vol. 5869. SPIE; 2005. p. 58691D.

[12] Werling S, Mai M, Heizmann M, Beyerer J. Inspection of specular and partially specular surfaces. Metrol Meas Syst 2009;16(3):415–31.

[13] Balzer J, Werling S. Principles of shape from specular reflection. Measurement 2010;43(10):1305–17. https://doi.org/10.1016/j.measurement.2010.07.013.

[14] Häusler G, Faber C, Olesch E, Ettl S. Deflectometry vs. Interferometry. In: Lehmann PH, Osten W, Albertazzi A, editors. Optical measurement systems for industrial inspection VIII. International society for optics and photonics, vol. 8788. SPIE; 2013. p. 87881C.

[15] Huang L, Xue J, Gao B, McPherson C, Beverage J, Idir M. Modal phase measuring deflectometry. Opt Express 2016;24(21):24649–64. https://doi.org/10.1364/OE.24.024649. https://opg.optica.org/oe/abstract.cfm?URI=oe-24-21-24649.

[16] Thorlabs. Telecentric lenses tutorial. https://www.thorlabs.com/newgrouppage9.cfm?objectgroup_id=10762, 2024.

[17] Zhimuleva ES, Zavyalov PS, Kravchenko MS. Development of telecentric objectives for dimensional inspection systems. Optoelectron Instrum Data Process 2018;54(1):52–60. https://doi.org/10.3103/S8756699018010090.

[18] Ansys, Zemax OpticStudio. https://www.ansys.com/products/optics/ansys-zemax-opticstudio, 2024.

[19] Bradski G. The OpenCV library. Dr Dobb's J Softw Tools 2000.

[20] Edmund Optics. Metallic mirror coatings. https://www.edmundoptics.com/knowledge-center/application-notes/optics/metallic-mirror-coatings, 2024.

[21] Edmund Optics. Anti Reflect (AR) Coatings 2024. https://www.edmundoptics.com/knowledge-center/application-notes/lasers/anti-reflection-coatings/.

[22] Huang L, Wang T, Austin C, Kim D, Idir M. Two-step retrace error calibration removing tilt ambiguity in coherence scanning interferometry. Opt Lett 2024;49(3):590–3. https://doi.org/10.1364/OL.510943. publisher: Optica Publishing Group. https://opg.optica.org/ol/abstract.cfm?uri=ol-49-3-590.